JOURNAL OF GEOPHYSICAL RESEARCH, VOL. 112, A08213, doi:10.1029/2007JA012357, 2007

Cluster observations in the inner magnetosphere during the 18 April 2002 sawtooth event: Dipolarization and injection at $r = 4.6\ R_E$

S. Ohtani,[1] H. Korth,[1] P. C. Brandt,[1] L. G. Blomberg,[2] H. J. Singer,[3] M. G. Henderson,[4] E. A. Lucek,[5] H. U. Frey,[6] Q. Zong,[7] J. M. Weygand,[8] Y. Zheng,[1] and A. T. Y. Lui[1]

Received 19 February 2007; revised 10 April 2007; accepted 21 May 2007; published 31 August 2007.

[1] The present study examines a sawtooth injection event that took place around 0800 UT on 18 April 2002 when the Cluster spacecraft were located in the inner magnetosphere in the premidnight sector. In association with this injection, Cluster, at a radial distance of 4.6 R_E, observed that the local magnetic field became more dipolar and that both ion and electron fluxes increased without notable energy dispersion. These features were accompanied by intensifications of the equatorward component of a double-oval structure and also by an enhancement of the ring-current oxygen ENA flux. The event was also accompanied by large magnetic field (a few tens of nT) and electric field (a few tens of mV/m) fluctuations with characteristic timescales of a few tens of seconds. These observations strongly suggest that this sawtooth injection extended not only widely in local time but also deeply into the inner magnetosphere. Interestingly, Cluster repeatedly observed dipolarization-like signatures afterward, which, however, were not associated with enhancements of local energetic ion flux or with geosynchronous dipolarization or injection signatures. Instead, these magnetic signatures were accompanied by oscillatory plasma motion in the radial direction with a characteristic timescale of about 10 min, which appears to be related to the westward propagation of a spatially periodic auroral structure. The associated azimuthal electric field component was well correlated with the time derivative of the north-south magnetic field component, suggesting that the observed electric field is inductive. These findings suggest that electromagnetic processes far inside geosynchronous orbit play an important role in energization of energetic ions and auroral dynamics during magnetospheric storms.

Citation: Ohtani, S., et al. (2007), Cluster observations in the inner magnetosphere during the 18 April 2002 sawtooth event: Dipolarization and injection at $r = 4.6\ R_E$, *J. Geophys. Res.*, *112*, A08213, doi:10.1029/2007JA012357.

1. Introduction

[2] Sawtooth injections are defined as repetitive occurrences of gradual decreases and successive sudden increases of energetic particle flux at geosynchronous altitude. The geosynchronous magnetic field dipolarizes at each injection. Whereas both injection and dipolarization are common substorm-related features observed in the nightside geosynchronous region, they are observed in an unusually extended local time range during sawtooth events. Associated injections are often observed over the entire nightside geosynchronous region and occasionally even on the dayside.

[3] The April 2002 storm event has been examined extensively because sawtooth injections were observed throughout 18 April 2002 during its main phase [*Huang*, 2002; *Reeves et al.*, 2002; *Lee et al.*, 2004; *Lui et al.*, 2004; *Kitamura et al.*, 2005; *Henderson et al.*, 2006; *Clauer et al.*, 2006]. For one of the injection events, which took place around 0800 UT, the Cluster constellation was located in the inner magnetosphere near perigee, crossing the magnetic equator from the southern to the northern hemisphere at an equatorial distance of 4.6 R_E in the premidnight sector [*Vallat et al.*, 2004]. During this injection event four geosynchronous satellites, two GOES and two LANL satellites, were located on the nightside. In addition, the IMAGE satellite was at a northern polar vantage point taking FUV auroral images and energetic neutral atom (ENA) images of the ring current.

[4] This fortuitous coordination of satellites allows us to comprehensively examine this sawtooth injection event. Sawtooth injections have been examined mostly with geosynchronous data, and in situ observations of sawtooth injections in the inner magnetosphere have been reported

[1]Johns Hopkins University Applied Physics Laboratory, Laurel, Maryland, USA.
[2]Royal Institute of Technology, Stockholm, Sweden.
[3]NOAA Space Environment Center, Boulder, Colorado, USA.
[4]Los Alamos National Laboratory, Los Alamos, New Mexico, USA.
[5]Blackett Laboratory, Imperial College, London, UK.
[6]Space Sciences Laboratory, University of California, Berkeley, California, USA.
[7]Center for Atmospheric Research, University of Massachusetts Lowell, Lowell, Massachusetts, USA.
[8]Institute of Geophysics and Planetary Physics, University of California, Los Angeles, California, USA.

0148-0227/07/2007JA012357$09.00

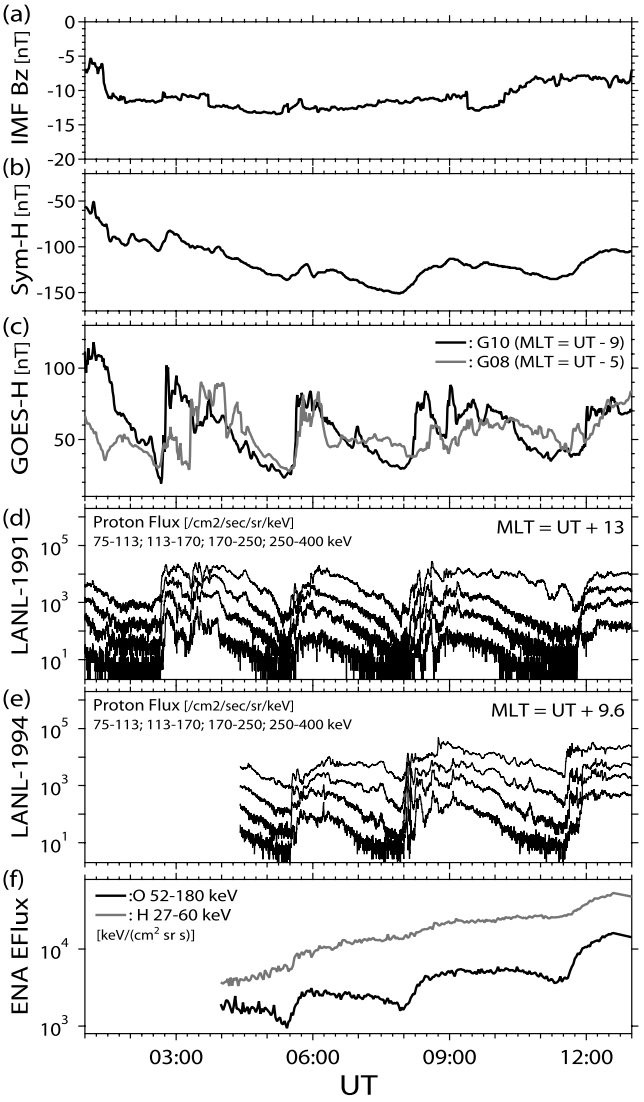

Figure 1. Summary of the 18 April 2002 sawtooth event. (a) The time-shifted IMF B_Z component in GSM measured by the ACE satellite (see *Weimer et al.* [2003] for the calculation of the propagation time), (b) the Sym-*H* index, (c) The *H* magnetic component observed by the GOES 8 (gray) and 10 (black) satellites, (d) 1991−080 and (e) 1994-084 measurements of energetic proton fluxes, and (f) image integrated 52−180 keV oxygen (black) and 27−60 keV hydrogen (gray) ENA fluxes.

for only a very few events [*Henderson*, 2004]. However, the energy density of the nightside ring current peaks far inside geosynchronous orbit, L = 3 ∼ 5, at storm time [*Smith and Hoffman*, 1973; *Krimigis et al.*, 1985; *Korth and Thomsen*, 2001; *Ebihara et al.*, 2002], and therefore addressing Cluster observations in the inner magnetosphere from the viewpoint of global magnetospheric and auroral dynamics is expected to shed new light not only on sawtooth injections but also on storm dynamics in general.

[5] In the present study we examine this sawtooth event with a focus on Cluster observations in the inner magnetosphere. In section 2 we briefly review the event and then examine auroral signatures with special attention to the sawtooth injection around 0800 UT. In section 3 we examine in detail magnetic field, electric field, and energetic ion signatures observed by the Cluster spacecraft and address them in the context of other satellite observations and auroral features. Results are discussed in section 4. Section 5 is a summary.

2. Sawtooth Event of 18 April 2002

2.1. Overview

[6] Sawtooth injections took place on 18 April 2002 during a magnetospheric storm, which followed a storm sudden commencement at 1106 UT on the previous day. This is a two-step storm event [*Kamide et al.*, 1998]. The *Sym-H* index reached its first minimum, −151 nT, at ∼0800 UT on 18 April 2002. The *Sym-H* minimum of the entire storm interval, −185 nT, took place at ∼0600 UT on 20 April 2002.

[7] Figure 1 shows key observations for the 12-hour interval from 0100 to 1300 UT on 18 April 2002 around the first *Sym-H* minimum. The IMF B_Z component was continuously southward (Figure 1a), and *Sym-H* decreased until about 0800 UT (Figure 1b). During this 12-hour interval LANL geosynchronous satellites, 1991-080 and 1994-084, observed four injections in the afternoon-to-midnight region (Figures 1d and 1e), each of which was accompanied by dipolarization as indicated by increases in the geosynchronous *H* (north-south) component observed by GOES satellites (Figure 1c) [*Reeves et al.*, 2002; *Henderson et al.*, 2006]. *Sym-H* recovered temporarily following each injection/dipolarization, which is likely due to the associated reduction of the tail current intensity rather than to the decay of the ring current [*Siscoe and Petschek*, 1997; *Ohtani et al.*, 2001, 2005]; see *Kitamura et al.* [2005] and *Clauer et al.* [2006] concerning the ground magnetic disturbances associated with these sawtooth injections.

[8] The energy flux of the 52−180 keV oxygen ENA flux measured by the IMAGE/HENA instrument [*Mitchell et al.*, 2000] also enhanced simultaneously with the injections/dipolarizations (Figure 1f, black trace). Here we integrated the ENA flux within 54° in both azimuth and elevation centered at Earth for every 2-min image; the area is large enough to cover the entire ring current region. In contrast, the associated enhancement of the 27−60 keV hydrogen ENA (gray trace) was not pronounced, although there are suggestive changes of the slope. It is common that the oxygen ENA flux increases more significantly than the hydrogen ENA flux at substorm onsets [*Mitchell et al.*, 2003; *Ohtani et al.*, 2005]. Note that the overall increasing trend of the ENA flux can be attributed at least partly to the inbound motion of the IMAGE satellite; the satellite moved from (−4.7, 0.9, 5.1) to (1.9, 0.2, 3.0) R_E in GSM coordinates during the 12-hour interval shown in Figure 1.

2.2. Auroral Dynamics

[9] The IMAGE/WIC instrument [*Mende et al.*, 2000] observed the northern polar region for the early half of 18 April 2002, taking auroral images in approximately 2-min time steps. Figure 2a shows selected images taken between 0745 and 1002 UT, remapped into the Altitude Adjusted Corrected Geomagnetic (AACGM) Coordinate system [*Baker and Wing*, 1989]. Note that these images

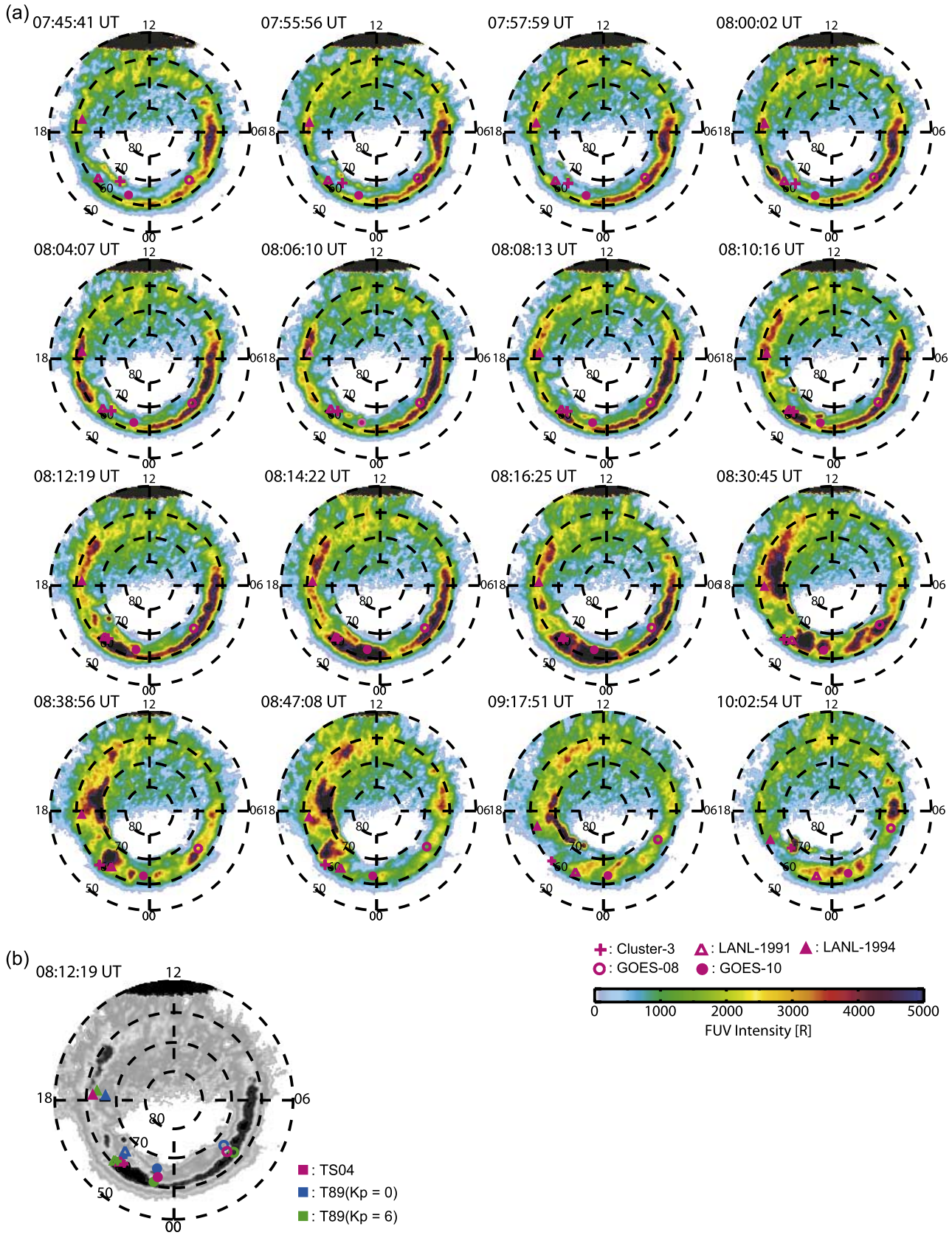

Figure 2. (a) Selected auroral images taken by IMAGE/WIC for 0745:4–1002:54 UT on 18 April 2002. Satellite footpoints are marked by different marks. (b) Satellite footpoints calculated by different magnetic field models for the image of 0812:19 UT.

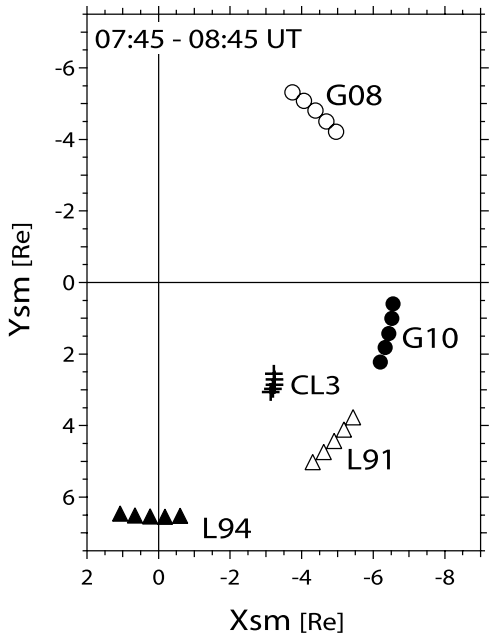

Figure 3. Positions of the Cluster 3 (CL3), GOES 8 (G08), 10 (G10), 1991-080 (L91), and 1994-084 (L94) satellites in the *X*-*Y* SM plane.

are not equally separated in time. The various plot symbols denote magnetic footpoints of the geosynchronous and Cluster 3 satellites calculated with the TS04 model [*Tsyganenko and Sitnov*, 2005] using actual solar wind and IMF data time-shifted to Earth. The WIC instrument takes images with an exposure period of 24 s and each frame is labeled with the start time of the exposure.

[10] To assess the field-line mapping uncertainty, we also calculated the footpoint of each satellite with the T89 model [*Tsyganenko*, 1989] parameterized by Kp = 0 and 6. The results are shown in Figure 2b in different colors (blue for T89 Kp = 0 and green for T89 Kp = 6) for one example snapshot taken at 0812 UT. As Kp increases from 0 to 6, the footpoint moves equatorward by as much as 5° for geosynchronous satellites. Since the actual Kp index was 6- during the interval, the T89 Kp = 6 model is expected to be closer to the actual magnetic configuration. In fact, we will later find that the local magnetic field at Cluster was significantly more stretched than the T89 Kp = 0 model predicts. The TS04 model tends to map the satellite positions slightly poleward and closer to midnight than the T89 Kp = 6 model.

[11] On the nightside the auroral distribution showed a double-oval structure during this sawtooth event [*Henderson et al.*, 2006]. Whereas the poleward oval often became faint, the equatorward oval was continuously active, revealing many temporal and spatial features. New auroral activity started around 0758 UT in the late evening sector around 21.5 MLT near the footpoint of 1991-080 (Figure 2). A bulge developed immediately and expanded mostly westward. Its eastward expansion, if at all present, was limited. Although the intense emission region propagated continuously westward, the overall auroral intensity weakened rapidly. Distinct auroral activity started around 0806 UT at ~22.5 MLT, to the east of the first activity, which cannot

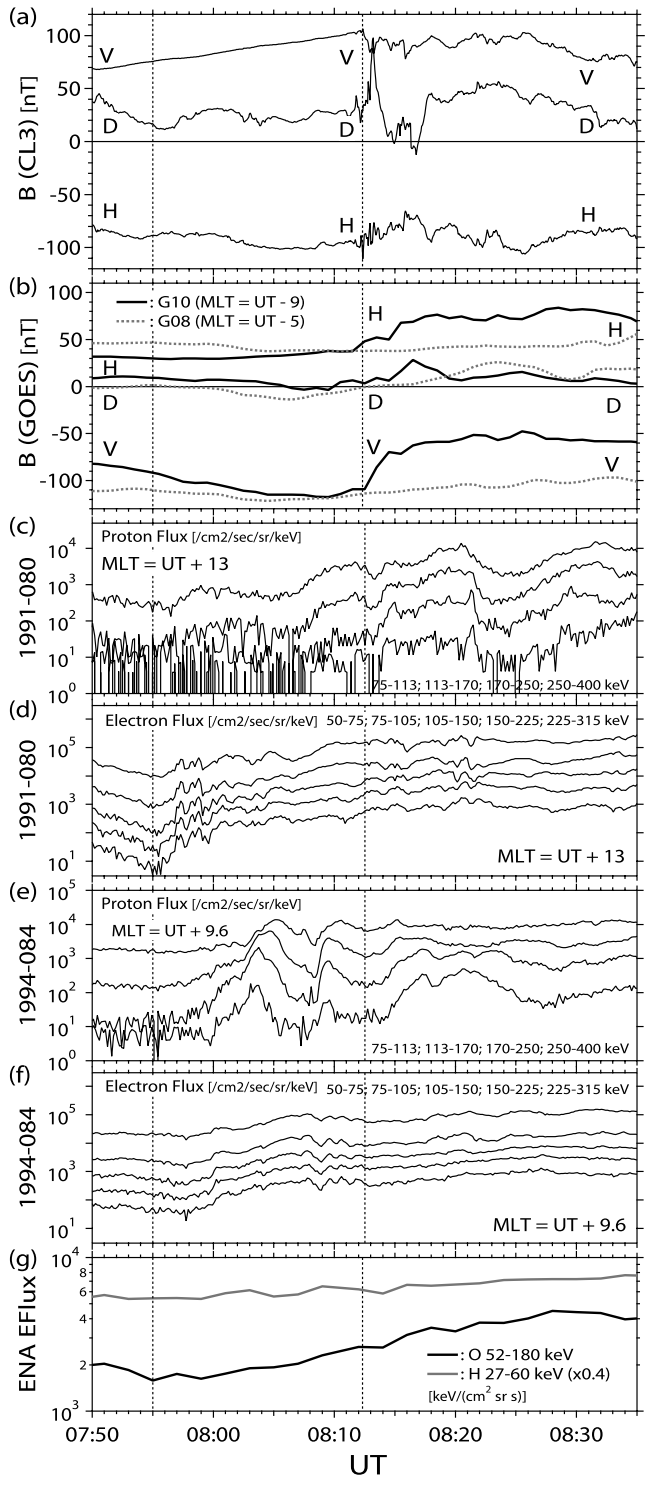

Figure 4. (a) Cluster-3, (b) GOES 8 (dashed) and 10 (solid) magnetic field measurements, 1991-080 (c) energetic proton and (d) electron flux measurements, 1994-084 (e) energetic proton and (f) electron flux measurements, and image-integrated 52–180 keV oxygen (black) and 27–60 keV hydrogen (gray) ENA fluxes for 0750–0835 UT on 18 April 2002.

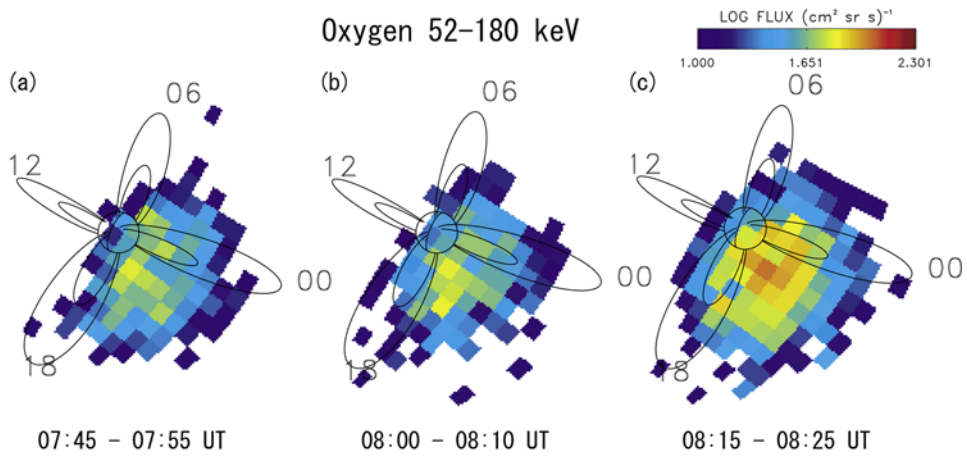

Figure 5. Energetic (52–180 keV) oxygen ENA images taken by IMAGE/HENA for (a) 0745–0755, (b) 0800–0810, and (c) 0815–0825 UT on 18 April 2002. The IMAGE satellite was around (−3, 2, 7) R_E in SM. Images taken at four energy channels ranging from 52 to 180 keV are combined and are averaged over each interval. The circle at the center represents the Earth, and also shown are L = 4 and 8 dipole field lines at four local times.

be recognized in the preceding image of 0804 UT. The bulge expanded westward and eastward as well as poleward. The eastward expansion was noticeably faster than the westward expansion. As the bulge faded out, bright auroral spots emerged, which were distributed quasi-periodically in local time (e.g., see the image taken at 0838:56 UT in Figure 2). In contrast, in the postmidnight-to-morning sector, the auroral oval was stable during the course of these successive events although the auroral emission was continuously intense.

2.3. Sawtooth Injection Around 0800 UT

[12] In this subsection we briefly examine the sawtooth injection around 0800 UT. Figure 3 shows the positions of geosynchronous satellites and Cluster 3 in SM *X-Y* coordinates in 15 min steps from 0745 to 0845 UT. GOES 8 and 10 were located in the early morning and premidnight sectors, respectively. The 1991-080 and Cluster 3 were located in the late evening sector, and 1994-084 was at dusk.

[13] Figure 4 shows magnetic field and energetic particle fluxes measured by those satellites for 0750-0835 UT along with the image-integrated ENA fluxes of the 27–60 keV hydrogen and 52–180 keV oxygen. The magnetic field data are presented in the *VDH* coordinate system; *H* is parallel to the dipole axis and is positive northward, *V* points radially outward and is parallel to the magnetic equator, and *D* completes a right-hand orthogonal system and is positive eastward. The centered dipole plus T89 (Kp = 0) model field is subtracted from the Cluster magnetic field observations. The vertical dashed line marks 0812:20 UT, when the local magnetic field became more dipolar at Cluster 3 as indicated by the increase in *H* and decrease in *V* (Figure 4a). The Cluster observations will be examined in more detail in section 3.

[14] Simultaneously with, or slightly earlier than Cluster 3, GOES 10 also observed dipolarization as indicated by an increase in *H* and a decrease in $|V|$ (solid lines in Figure 4b). In contrast, GOES 8, located in the dawn sector, did not observe any dipolarization signature (dotted lines in Figure 4b). This is consistent with the fact that the auroral oval was stable from the postmidnight-to-morning sector even though the auroral intensity was continuously enhanced (section 2.2).

[15] Both 1991-080 and 1994-084 observed enhancements of energetic particle fluxes, which started noticeably earlier than the dipolarization at the Cluster 3 and GOES 10 locations. At 1991-080 energetic electron fluxes started to increase at 0755 UT (Figure 4d), and the 75-133 keV proton flux increased 2 min later, whereas the count rates for higher-energy protons are too low to specify the timing of the flux enhancement (Figure 4c). At 1994-084 the increase of energetic electron and proton fluxes started around 0759 UT, and the proton fluxes revealed energy dispersion (Figures 4e and 4f). We therefore infer that the associated injection started closer in MLT to 1991-080 than to 1994-084. Presumably this injection was associated with the auroral activity that started around 0758 UT near the footpoint of 1991-080 (Figure 2).

[16] The electron fluxes did not reveal any significant increase at either 1991-080 or 1994-084 after the initial rise at 0755 UT. In contrast, the proton fluxes increased at 1991-080 repetitively around 0807, 0813, and 0824 UT, and corresponding enhancements were also observed at 1994-084. Since protons drift westward and electrons drift eastward, we infer from these observations that the associated injection region moved to the east of 1991-080. This is consistent with the fact that new auroral activity started at 0806 UT at MLT $\sim$ 2200, to the east of the previous auroral activity (Figure 2). Thus this sawtooth injection consisted of at least two distinct events that took place in different locations but close to each other in time.

[17] As mentioned in section 2.1, the image-integrated ENA flux of the 27–60 keV hydrogen did not change significantly. In contrast, the 52–180 keV oxygen ENA flux

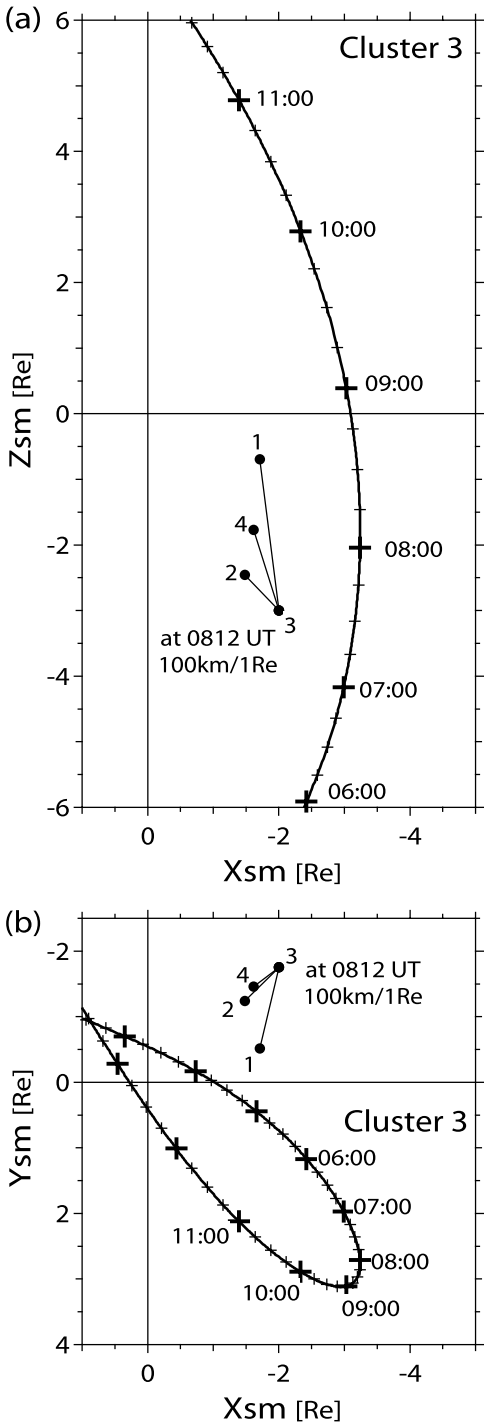

Figure 6. Positions of the Cluster 3 satellite in the (a) *X-Z* and (b) *X-Y* SM planes. The inserts show the relative locations of the other three Cluster satellites (as identified by the satellite numbers) to Cluster 3 at 0812 UT on a different scale (100 km/1 R_E).

started to increase before 0800 UT (Figure 4g), presumably corresponding to the first auroral intensification and geosynchronous injection, and it continued to increase through the successive intensification at 0806 UT. Figure 5 shows oxygen ENA images averaged over three 10-min intervals, 0745–0755, 0800–0810, and 0815–0825 UT. The first auroral intensification took place between the first and second 10-min intervals, and the second intensification during the second 10-min interval. Dipolarization at Cluster took place between the second and third intervals. The effective angular resolution of the oxygen ENA measurement is as large as 20° [*Mitchell et al.*, 2003], which corresponds to about 3 R_E in an image taken at 8 R_E from Earth, the radial distance of the IMAGE satellite during those intervals. Thus caution needs to be exercised when addressing the source location of the flux. Nevertheless, it is plausible that the enhancement of the oxygen ENA flux took place mostly in the dusk-to-midnight sector, where those two auroral activations took place, and Cluster was located in that sector.

3. Cluster Observations

3.1. Cluster Observations Along the Perigee Pass

[18] The Cluster mission [*Escoubet et al.*, 2001] consists of four identical satellites, which fly in formation at varying separation distances. In the present study we will primarily examine measurements made by the Cluster 3 satellite and will refer to other Cluster satellites when appropriate. Figures 6a and 6b show the orbit of Cluster 3 on 18 April 2002 in the SM *X-Z* and *X-Y* planes, respectively. The spacecraft was on a perigee pass moving from the southern to the northern hemisphere in the premidnight sector. The perigee distance of Cluster is 4.0 R_E. The diagram inserted in Figures 6a and 6b shows the relative locations of the other Cluster satellites at 0812 UT, which are identified by number. The scale factor for the interspacecraft separation in the plot is 100 km per 1 R_E. The maximum separation among the spacecraft was a few hundred kilometers throughout the interval.

[19] Figure 7 shows measurements made by the Cluster 3 magnetometer [*Balogh et al.*, 2001] (solid line) together with the quiet time (Kp = 0) T89 model field at the position

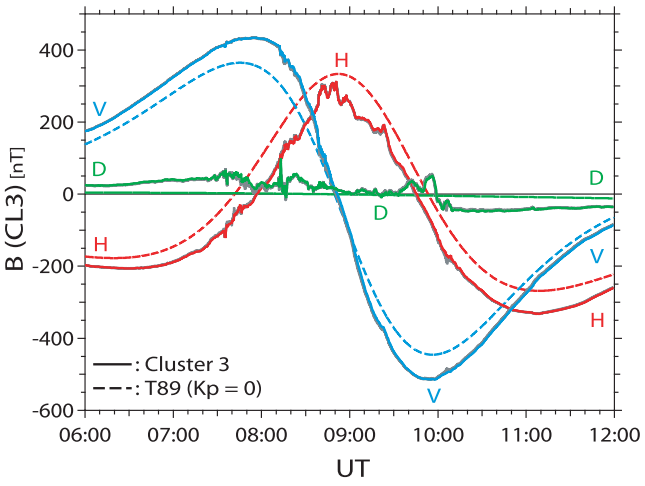

Figure 7. The *V*(blued), *D*(green), and *H*(red) magnetic components measured by Cluster 3 (solid) along with the T89 (Kp = 0) model field (dashed) at the Cluster 3 position for 0600–1200 UT on 18 April 2002. Data from other Cluster satellites are also plotted by gray lines underneath, which, however, are barely distinguishable.

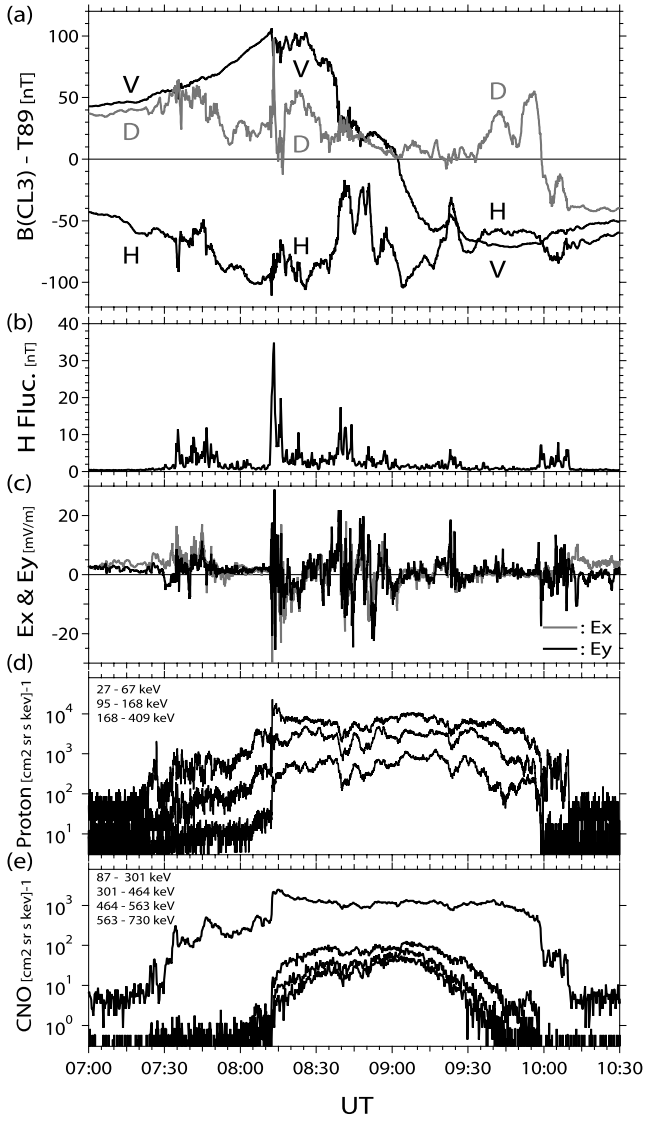

Figure 8. Cluster 3 measurements of (a) *V*, *D*, and *H* magnetic components after subtraction of the T89 (Kp = 0) model, (b) the peak-to-peak amplitude of the detrended *H* magnetic component for 20 s, (c) the *X* and *Y* electric field components in spacecraft coordinates, (d) energetic proton fluxes, and (e) heavy ion fluxes for 0700–1030 UT on 18 April 2002.

of Cluster 3. We use the Kp = 0 version of the model to exhibit the storm time deviations. Data from the other three Cluster satellites are also plotted in gray, which, however, are difficult to identify because they follow the traces of Cluster 3 data closely. In general, the observation follows the model field. However, the *H* component is consistently depressed from the model field, which can be attributed to the intensification of the ring current and tail current during this storm event. The magnitude of the observed *V* component is generally larger than that of the model *V* component indicating that the magnetic field was stretched in the inner magnetosphere. The magnitude of the *D* component was relatively small throughout the interval; that is, the magnetic field lay approximately in the magnetic meridional plane. The sign of the *V* component changes at 0852 UT when the *H* component was near its peak, indicating the crossing of the geomagnetic equator. The satellite was indeed close to the *X*-*Y* SM plane then and its radial distance was 4.4 R_E (Figure 3a).

[20] While the traces of the model field in Figure 7 are smooth, the observations show many fluctuations. Figure 8a plots the difference between the observed and quiet time T89 magnetic components for a portion (0700–1030 UT) of the interval shown in Figure 7. To assess the level of fluctuations in the *H* component on short timescales, we fit a straight line to the 22-Hz *H* component measurements in 20-s segments every 10 s and calculated the difference between the maximum and minimum of deviations from the fit, which is plotted in Figure 8b. In Figure 8c we plot the *X* and *Y* components of the electric field in the spacecraft coordinate system, which for all practical purposes can be considered the GSE system [*Gustafsson et al.*, 2001]. Figures 8d and 8e show the fluxes of energetic protons and heavy ions (carbon, nitrogen, and oxygen ions: CNO) observed by the RAPID instrument, respectively [*Wilken et al.*, 2001]; for the CNO flux, oxygen is the dominant component [*Christon et al.*, 2002]. Note that the lowest-energy CNO channel (87–301 keV) covers the core energy range of the ring current ions, whereas the remaining three channels cover above 300 keV and accordingly follow a trend different from that seen in the lowest energy channel.

[21] Large magnetic variations were observed between 0720 and 1010 UT, the interval which coincides with the flux enhancements of the lowest-energy proton and oxygen channels. We infer that the spacecraft was in the closed field-line region during this interval. From plasma (<40 keV) ion measurements *Vallat et al.* [2004] identified the corresponding region as the plasma sheet (and the ring current further inside), which is consistent with our interpretation. These authors examined plasma data from Cluster 4, which was only a few hundred kilometers away from Cluster 3 and observed nearly identical magnetic field signatures (see also Figure 7).

[22] As the spacecraft entered the closed field-line region, the *D* component decreased during 0740–0755 UT following a gradual increase. The *D* component also decreased, but more sharply, after 1000 UT, when the spacecraft exited from the closed field-line region. The corresponding features were observed by the other Cluster satellites (Figure 7). The timing study shows that at each decrease in the *D* component the associated FAC structure moved southward relative to the Cluster constellation (not shown), from which we infer that these *D*-component decreases can be attributed to the satellite crossing a field-aligned current (FAC) sheet and that the associated FAC was flowing out of the ionosphere. This FAC polarity is the same as that of the R1 current in the premidnight sector. The upward FACs, which were observed both at entry to and at exit from the plasma sheet, map to the poleward component of the double-oval structure (see the frames of 0745:41 and 1002:54 UT in Figure 2). The latter one maps to near the localized bright auroral spot, which explains why the FAC was far more intense at the exit than it was at the entry into the plasma sheet.

[23] Magnetic variations in the middle of the interval were observed deep inside the closed field-line region.

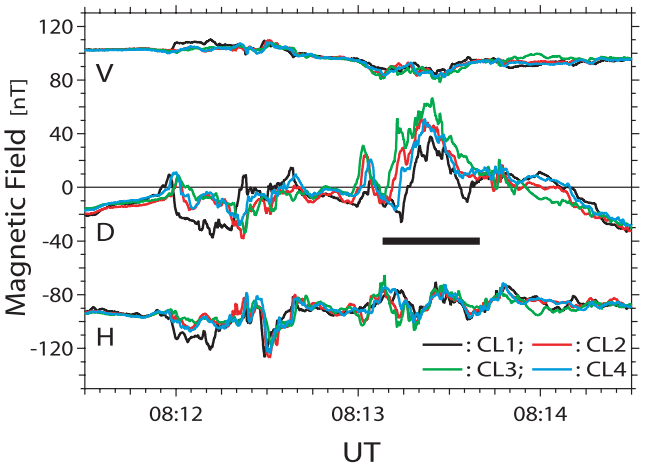

Figure 9. Full time-resolution (22 Hz) magnetometer data acquired by Cluster 1 (black), 2 (red), 3 (green), and 4 (blue) for 0811:30–0814:30 on 18 April 2002. The T89 (Kp = 0) model field at each satellite is subtracted. The interval of the positive D spike is marked by the horizontal bar.

At 0812 UT, in the middle of the sawtooth injection (section 2.3), the energetic proton fluxes increased sharply (Figure 8d), accompanied by an increase in H and a decrease in V (and in $|V|$). That is, the local magnetic field changed from a stressed to a more dipolar configuration (Figures 4a and 8a). These particle and magnetic signatures appear to be the same phenomena as dispersionless injection and dipolarization often observed at geosynchronous orbit, but Cluster 3 was much closer to Earth ($r \sim 4.6\ R_E$).

[24] The oxygen fluxes also increased simultaneously with the local dipolarization (Figure 8e), which took place in the middle of the oxygen ENA flux enhancement (section 2.3). We therefore consider that the associated oxygen ion energization took place on a rather large spatial scale. Whereas the oxygen ion flux increased within one minute at Cluster 3, the enhancement of the oxygen ENA flux was gradual and continued for almost 30 min (Figure 4g). This suggests that Cluster observed the flux enhancement as the energization/injection region expanded.

[25] The location of Cluster 3 maps to the ionosphere to the west of the second auroral intensification region; see the frames at 0806:10 and 0808:13 UT in Figure 2. It is therefore suggested that Cluster 3 observed the local dipolarization as the associated activity (dipolarization) region expanded westward. This idea is supported by the large (~80 nT) positive spike in the D component observed by Cluster 3 at the start of the local dipolarization. Figure 9 plots magnetic field measurements made by all four Cluster spacecraft for the 3-min interval, 0811:30–0814:30 UT, around the start of the dipolarization. Full time resolution (22 Hz) data are used. The positive D spike started first at Cluster 3 at 0813:08 UT and subsequently at Cluster 2, 4, and 1, in order of decreasing distance from the SM equatorial plane (Figure 6), and the order for the D decrease appears to be the opposite among the four spacecraft although it is less clear. This suggests that a FAC sheet moved initially equatorward and then poleward in association with the positive D spike, and accordingly the polarity of the FAC is inferred to be upward. That is, the associated FAC was flowing out of the ionosphere, and it was presumably related to the aforementioned auroral bulge.

[26] The increase of the H component was also observed at 0838 and 0917 UT (Figure 8a). However, an associated particle flux enhancement, if at all, was unclear. At 0838 UT, the H component increased by 80 nT and the V component decreased by 60 nT within 5 min. This sharp configurational change is presumably related to a bright auroral spot that passed the meridian of the Cluster 3 footpoint as it moved westward (see the frames at 0830:45, 0838:56, and 0847:08 UT in Figure 2). In contrast, we could not find any auroral feature that corresponds to the H increase at 0917 UT (see the frame at 0917:51 UT of Figure 2) despite detailed analysis of the auroral images. The aurora intensified along the poleward oval in the Cluster MLT sector, but it is rather difficult to associate it with the H increase at Cluster 3, which maps to the ionosphere almost 10° equatorward. Furthermore, in contrast to the 0812 UT event, no corresponding feature was observed at geosynchronous orbit although the other Cluster satellites observed the same dipolarization-like signature (Figure 7). Thus we infer that this H increase was caused by a change of the local current that was so confined in space that its effect was observed only by the Cluster spacecraft.

[27] The 0812 UT dipolarization may also be distinguished in terms of the level of magnetic field fluctuations. Although the H increase itself was smaller in magnitude in the 0812 UT event than in the later events, short-timescale magnetic fluctuations were significantly larger in the 0812 UT event (Figure 8b). For the 0812 UT event the H component varied with a characteristic timescale of a few tens of seconds (Figure 9), and the peak-to-peak amplitude exceeded 20 nT. Such fluctuations were unclear for the other events (not shown). The amplitude of electric field fluctuations were also large in the 0812 UT event (Figure 8c), and the fluctuations had shorter characteristic timescale, a few tens of seconds, than in the later events. These fluctuations may be manifestations of the change of the local current intensity. In general, the observed magnetic signatures were similar among the four Cluster spacecraft, but some differences are noticeable (Figure 9). This suggests that the characteristic spatial scale of the associated current change was larger than the spacecraft separation (~100 km), but it has some internal structures.

3.2. Comparison Between Electric and Magnetic Field Measurements

[28] In this subsection we compare magnetic field and electric field measurements made by Cluster 3 with a focus on long-timescale (>10 min) variations rather than short-timescale (a few tens of seconds) variations that we addressed above. Since the electric field is measured in the satellite spin plane, which is approximately aligned with the X-Y GSE plane, we transform the magnetic field data into the GSE coordinate system. Figure 10 plots, from the top, 30-s averages of B_Z, $\partial B_Z/\partial t$, the azimuthal (E_ϕ; positive eastward) and radial (E_r; positive outward) electric field components for 0800–0930 UT. As before, the T89 model (Kp = 0) magnetic field is subtracted from the magnetic

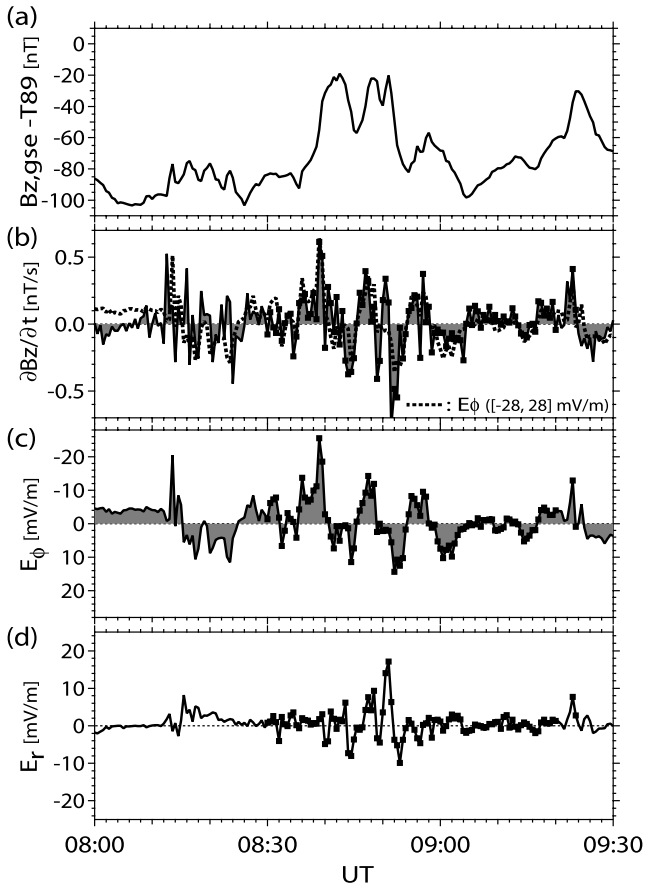

Figure 10. Thirty-second averages of Cluster 3 measurements of (a) the GSE Z magnetic component, (b) its time derivative, (c) the azimuthal (positive eastward but with the vertical axis inverted) and (d) radial (positive outward) electric field components in the GSE X-Y plane for 0800–0930 UT on 18 April 2002. The dots mark data points where the magnetic field is within 60° of the GSE Z axis.

field measurements, and $\partial B_Z/\partial t$ is calculated with the B_Z values after subtraction. From the observed electric field we subtracted the induction field resulting from the satellite motion, which is on the order of 1 mV/m (for example, for a magnetic field strength of 200 nT and a cross-field satellite velocity of 5 km/s). The vertical axis is inverted for E_ϕ (Figure 10c) for easier comparison with $\partial B_Z/\partial t$.

[29] There are three points to be noted regarding the electric field variations. First, E_ϕ (Figure 10c) is generally larger than E_r (Figure 10d) in magnitude indicating that the electric field is mostly azimuthal, and therefore the electric drift is in the radial direction. Second, E_ϕ is surprisingly large (even though it is averaged over 30 s), and it occasionally exceeds 10 mV/m. Note that an electric field of 10 mV/m, if static, corresponds to a potential difference of 60 kV over 1 R_E; we will, however, soon find that the observed electric field is mostly inductive. In contrast, the average dawn-to-dusk electric field around $L \sim 4.5$ is of the order of 1 mV/m even at high (>5) Kp levels [*Rowland and Wygant*, 1998]. Finally, E_ϕ alters its sign quasi-periodically indicating that the plasma oscillated in the radial direction at a characteristic period of 10 min. We regard this E_ϕ variation as a temporal effect. Note that the satellite moved only 0.5 R_E mostly in the Z direction (Figure 3), and if the signature is spatial, the associated structure would consist of many layers of positive and negative E_ϕ with magnitudes of ~10 mV/m, which we think is highly unlikely.

[30] Compared to E_ϕ, the variation of $\partial B_Z/\partial t$ has high-frequency components (Figure 10b). Nevertheless, these two quantities, actually $-E_\phi$ and $\partial B_Z/\partial t$, changed in time in a similar way; the dotted line in Figure 10b shows $-E_\phi$, which is the same as plotted in Figure 10c. Figure 11 plots E_ϕ against $\partial B_Z/\partial t$ for data points when the magnetic field is within 60° of the GSE Z axis. The corresponding data points are denoted by dots in Figure 10. The fitted line represents the result of the linear regression analysis. The two quantities are negatively correlated, with a correlation coefficient of −0.68, indicating that B_Z increases and decreases when the plasma moves earthward and tailward, respectively.

[31] The fact that E_ϕ and $\partial B_Z/\partial t$ are correlated also indicates that the observed electric field is inductive. The inductive electric field, $\vec{E}$ is described by the time derivative of the magnetic field, $\vec{B}$, by $\frac{\partial \vec{B}}{\partial t} = -\nabla \times \vec{E}$. Taking its Z component and using the slope of the fitted line in Figure 11, the characteristic scale of the $\vec{E}$ variation in the radial direction is estimated at 3 R_E. We emphasize that this estimate is only suggestive because we neglected the azimuthal derivative of E_r and assumed that $\partial E_\phi/\partial r$ makes the dominant contribution to $-\nabla \times \vec{E}$.

4. Discussion

[32] The Cluster spacecraft observed dipolarization of the local magnetic field and a simultaneous enhancement of

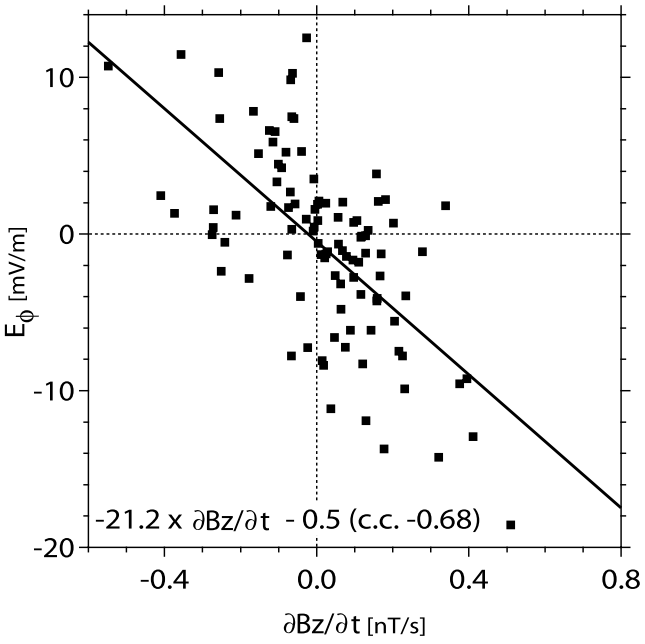

Figure 11. The azimuthal electric field component vs. the time derivative of the GSE Z magnetic components. Only data points with the magnetic field within 60° of the GSE Z axis (marked by dots in Figure 10) are used.

energetic ion fluxes at 0812 UT during the 18 April 2002 sawtooth event. These features appear to be the same phenomenon as the well-known geosynchronous dipolarization and injection often observed during substorms except that Cluster was located at 4.6 R_E from Earth, far inside geosynchronous orbit, where the occurrence of dipolarization is far less frequent than at geosynchronous orbit and farther radial distances [*Lopez et al.*, 1988]. This unusual location can be attributed to the intensified ring current (or the inward motion of the tail current) during this storm interval.

[33] In general, an increase in the *H* component is caused by the reduction of the tail current farther outside, and a dipolarization signature observed in the inner magnetosphere, such as observed by Cluster in the present event, could be a remote effect of tail current reduction that takes place farther away from Earth. Accordingly, the simultaneous increase in energetic ion flux observed by Cluster may be interpreted in terms of the satellite crossing a boundary, which we cannot specify except that it is not the plasma sheet boundary layer since the spacecraft was deep inside the closed field-line region. The difficulty of this idea, however, is that in the present event cluster 3 observed large-amplitude and highly irregular variations of the magnetic and electric fields at the time of dipolarization; the peak-to-peak amplitude of the *H* variation was as large as 50 nT and the magnitude of the electric field, even when spin-averaged, reached 40 mV/m at one point (Figure 8c). The characteristic timescale of these variations was a few tens of seconds, which is shorter than the MHD timescale of the inner magnetosphere, such as the period range of the Pi2 pulsation, 40–150 s. It seems unlikely that such large-amplitude high-frequency oscillations are effects of a process that occurred far from the spacecraft. We therefore suggest that the dipolarization and the increase of energetic ion fluxes observed by Cluster reflect a local process, which is likely the same as what is phenomenologically known as tail current disruption.

[34] The cause of dipolarization or the mechanism of tail current disruption is beyond the scope of the present study. Though, we would like to make two points based on the Cluster observation. First, the characteristic timescale of the embedded magnetic fluctuations, 20 s, is similar to that of magnetic fluctuations observed during current disruption events in the near-Earth region [*Ohtani et al.*, 1995]. It should, however, be noted that the background field was stronger at the Cluster position by more than an order of magnitude. Second, although near-Earth dipolarization is often addressed in terms of the pileup of magnetic flux carried from farther down the tail (by the fast flow created by near-Earth reconnection) [*Hesse and Birn*, 1991; *Shiokawa et al.*, 1998], it is not clear, and it may even be implausible, that such fast flows reach as close to Earth as the Cluster location in this event, $r \sim 4.6\ R_E$. Although the depression of the magnetic field owing to the intense ring current is favorable for this idea, the total magnetic field exceeded 200 nT when cluster crossed the equator (Figure 7); at the 0812 UT dipolarization Cluster was off the equator but *H* component, which may be used as a proxy of the equatorial magnetic field strength, was larger than 100 nT. Since the equatorial magnetic field in the midtail region is typically 10 nT or less, the fast flow needs to overcome an increase in the magnetic pressure by at least two orders of magnitude in order to reach the Cluster location.

[35] The most intriguing issue concerning the Cluster observation is why the energetic ion flux did not increase significantly when the local magnetic field became more dipolar later as it did at 0812 UT. The later events, especially the one at 0838 UT, consisted of larger magnetic changes. Note also that the oxygen ENA flux did not reveal any clear enhancement at those later events, whereas it increased for about 30 min following the initial auroral activation at 0758 UT (Figure 4g).

[36] One possibility is that the 0812 UT event was special and that the energetic ion flux increased simultaneously only because the spacecraft entered a different plasma region as the magnetic configuration changed. If this is the case, the energetic ion flux would not increase at later events simply because the spacecraft was already in that region. However, as mentioned earlier, we are not aware of any corresponding plasma boundary in the inner magnetosphere. One might think that the demarcation of open and closed trajectories may correspond to such a boundary. However, the drift trajectory depends on the energy and pitch angle of ions, and so does the location of the demarcation between open and closed trajectories. In fact, when Cluster exited from the closed field-line region, it observed the energetic ion fluxes to decrease distinctively for different species and energies. At 0812 UT, however, the fluxes of all ion species and energies increased simultaneously. Nevertheless, we are hesitant to disregard this idea mostly because we do not understand why the double oval forms especially during magnetospheric storms as it did in the present event or what separates the equatorward oval from the poleward one. If the equatorward oval is an ionospheric projection of some magnetospheric region deep inside the closed field-line region, it is possible that Cluster crossed the outer boundary of such a region at 0812 UT.

[37] An alternative idea is that the 0812 UT event was indeed dipolarization/injection and ions were accelerated locally at Cluster 3, whereas the later configurational changes were caused by large-scale oscillations of the inner magnetosphere. During the 0812 UT event Cluster observed large-amplitude magnetic and electric fluctuations, but such fluctuations were smaller and less clear in the later events even though the magnitudes of the configurational changes were larger than in the 0812 UT event. These fluctuations may distinguish the 0812 UT event from the later events. After the 0812 UT event the azimuthal electric field, E_ϕ, and therefore the radial electric drift, changed quasi-periodically. This supports the idea that the later configurational changes were large-scale oscillations of the inner magnetosphere. In such a case the change of the local magnetic field to a more dipolar configuration may not have to be accompanied by any significant energization of ions.

[38] The characteristic timescale of the azimuthal electric field oscillations, 10 min, is longer than the typical period of field line oscillations and that of Pi2 waves. Thus this quasi-periodic oscillation must be related to something that propagates or moves much slower than MHD waves, and we speculate that convection, or its shear, is a reasonable candidate. From that perspective, it is interesting to point out that the auroral emission had a quasi-periodic structure in the azimuthal direction, which appeared to move

westward. See, for example, the frame at 0838:56 UT in Figure 2, in which several bright spots can be found in the dusk-to-midnight sector. In fact, when Cluster observed a dipolarization(-like) signature at 0838 UT, its footpoint was very close to one such auroral spot as we pointed out earlier (section 3.1). As the corresponding structure moves in the magnetosphere, it may be observed as quasi-periodic magnetic and electric oscillations by spacecraft.

[39] In closing we emphasize that this discussions is all based on a single event, and it is an open question how often and under what conditions such an oscillatory motion takes place in the inner magnetosphere. It is interesting and important to examine electromagnetic and particle signatures in the inner magnetosphere during other magnetospheric storms and compare them with temporal and spatial auroral variations.

5. Summary

[40] In the present study we examined the sawtooth event that took place on 18 April 2002. We focused on the Cluster observations of the magnetic field, electric field, and energetic ion flux variations in the inner magnetosphere in the premidnight sector. The following is a summary of observational results:

[41] 1. The equatorward component of the double oval structure can be mapped to the ring current region far inside geosynchronous orbit.

[42] 2. In association with the sawtooth injection at ~0800 UT, the Cluster spacecraft observed at $r \sim 4.6\ R_E$ the local magnetic field become more dipolar and both proton and electron fluxes increase without clear energy dispersion. The energetic oxygen flux also increased sharply, which presumably corresponded to the enhancement of the oxygen ENA flux observed by IMAGE/HENA.

[43] 3. Following the 0812 UT event Cluster observed dipolarization-like signatures, without enhancement of energetic ion flux. These signatures were not associated with substorm onsets or auroral intensifications. Instead, they were accompanied by oscillatory plasma motion in the radial direction, which possibly corresponded to periodic auroral structures that propagated westward.

[44] 4. The quasi-periodic oscillation of the azimuthal electric field component at the Cluster satellite was correlated with the differentiated B_Z magnetic component, indicating that the observed electric field is mostly inductive.

[45] These results suggest that electromagnetic processes in the inner magnetosphere are important for local energization of energetic ions and auroral dynamics during magnetospheric storms.

[46] **Acknowledgments.** The *Sym-H* index was provided by T. Iyemori through the World Data Center for Geomagnetism, Kyoto, and the ACE/MFI data was provided by C. Smith. Work at JHU/APL was supported by NSF grants ATM0318173 and ATM-0302529 and by NASA grant NAG513491. Work at LANL was supported by NASA LWS/TR&T grant LWS04-0000-0152 and NSF grants ATM031817 and ATM-0302529.

[47] Amitava Bhattacharjee thanks Craig J. Pollock and Ramon Lopez for their assistance in evaluating this paper.

References

Baker, K. B., and S. Wing (1989), A new magnetic coordinate system for conjugate studies at high latitude, *J. Geophys. Res.*, *94*, 9139.

Balogh, A., et al. (2001), The Cluster magnetic field investigation: Overview of inflight performance and initial results, *Ann. Geophys.*, *19*, 1207.

Christon, S. P., U. Mall, T. E. Eastman, G. Gloeckler, A. T. Y. Lui, R. W. McEntire, and E. C. Roelof (2002), Solar cycle and geomagnetic N^{+1}/O^{+1} variation in outer dayside magnetosphere: Possible relation to topside ionosphere, *Geophys. Res. Lett.*, *29*(5), 1058, doi:10.1029/2001GL013988.

Clauer, C. R., X. Cai, D. Welling, A. DeJong, and M. G. Henderson (2006), Characterizing the 18 April 2002 storm-time sawtooth events using ground magnetic data, *J. Geophys. Res.*, *111*, A04S90, doi:10.1029/2005JA011099.

Ebihara, Y., M. Ejiri, H. Nilsson, I. Sandahl, A. Milillo, M. Grande, J. Fennell, and J. Roeder (2002), Statistical distribution of the storm-time proton ring current: POLAR measurements, *Geophys. Res. Lett.*, *29*(20), 1969, doi:10.1029/2002GL015430.

Escoubet, C. P., M. Fehringer, and M. Goldstein (2001), The Cluster mission, *Ann. Geophys.*, *19*, 1197.

Gustafsson, G., et al. (2001), First results of electric field and density observations by Cluster EFW based on initial months of operation, *Ann. Geophys.*, *19*, 1219.

Henderson, M. G. (2004), The May 2–3, 1986 CDAW-9C interval: A sawtooth event, *Geophys. Res. Lett.*, *31*, L11804, doi:10.1029/2004GL019941.

Henderson, M. G., G. D. Reeves, R. Skoug, M. F. Thomsen, M. H. Denton, S. B. Mende, T. J. Immel, P. C. Brandt, and H. J. Singer (2006), Magnetospheric and auroral activity during the 18 April 2002 sawtooth event, *J. Geophys. Res.*, *111*, A01S90, doi:10.1029/2005JA011111.

Hesse, M., and J. Birn (1991), On dipolarization and its relation to the substorm current wedge, *J. Geophys. Res.*, *96*, 19,417.

Huang, C.-S. (2002), Evidence of periodic (2–3 hour) near-tail magnetic reconnection and plasmoid formation: Geotail observations, *Geophys. Res. Lett.*, *29*(24), 2189, doi:10.1029/2002GL016162.

Kamide, Y., N. Yokokawa, W. Gonzalez, B. T. Tsurutani, I. A. Daglis, A. Brekke, and S. Masuda (1998), Two-step development of geomagnetic storms, *J. Geophys. Res.*, *103*, 6917.

Kitamura, K., H. Kawano, S. Ohtani, A. Yoshikawa, and K. Yumoto (2005), Local-time distribution of low and middle latitude ground magnetic disturbances at sawtooth injections of April 18–19, 2002, *J. Geophys. Res.*, *110*, A07208, doi:10.1029/2004JA010734.

Korth, A., and M. F. Thomsen (2001), Plasma sheet access to geosynchronous orbit: Generalization to numerical global field models, *J. Geophys. Res.*, *106*, 29,655.

Krimigis, S. M., G. Gloeckler, R. W. McEntire, T. A. Potemra, F. L. Scarf, and E. G. Shelley (1985), Magnetic storm of September 4, 1984: A synthesis of ring current spectra and energy densities measured with AMPTE/CCE, *Geophys. Res. Lett.*, *12*, 329.

Lee, D.-Y., L. R. Lyons, and K. Yumoto (2004), Sawtooth oscillations directly driven by solar wind dynamic pressure enhancements, *J. Geophys. Res.*, *109*, A04202, doi:10.1029/2003JA010246.

Lopez, R. E., A. T. Y. Lui, D. G. Sibeck, R. W. McEntire, L. J. Zanetti, T. A. Potemra, and S. M. Krimigis (1988), The longitudinal and radial distribution of magnetic reconfigurations in the near-Earth magnetotail as observed by AMPTE/CCE, *J. Geophys. Res.*, *93*, 997.

Lui, A. T. Y., T. Hori, S. Ohtani, Y. Zhang, X. Y. Zhou, M. G. Henderson, T. Mukai, H. Hayakawa, and S. B. Mende (2004), Magnetotail behavior during storm time "sawtooth injections," *J. Geophys. Res.*, *109*, A10215, doi:10.1029/2004JA010543.

Mende, S. B., et al. (2000), Far ultraviolet imaging from the IMAGE spacecraft. 2, Wideband FUV imaging, *Space Sci. Rev.*, *91*, 271.

Mitchell, D. G., et al. (2000), High energy neutral atom (HENA) imager for the Image mission, *Space Sci. Rev.*, *91*, 67.

Mitchell, D. G., P. C. Brandt, E. C. Roelof, D. C. Hamilton, K. C. Retterer, and S. Mende (2003), Global imaging of O+ from IMAGE/HENA, *Space Sci. Rev.*, *109*, 63.

Ohtani, S., T. Higuchi, A. T. Y. Lui, and K. Takahashi (1995), Magnetic fluctuations associated with tail current disruption: Fractal analysis, *J. Geophys. Res.*, *100*, 19,135.

Ohtani, S., M. Nosé, G. Rostoker, H. Singer, A. T. Y. Lui, and M. Nakamura (2001), Storm-substorm relationship: Contribution of the tail current to Dst, *J. Geophys. Res.*, *106*, 21,199.

Ohtani, S., P. C. Brandt, D. G. Mitchell, H. Singer, M. Nosé, G. D. Reeves, and S. Mende (2005), Storm-substorm relationship: Variations of the hydrogen and oxygen ENA intensities during storm-time substorms, *J. Geophys. Res.*, 110, A07219, doi:10.1029/2004JA010954.

Reeves, G. D., et al. (2002), Global "sawtooth" activity in the April 2002 geomagnetic storm, *Eos Trans. AGU*, *83*(47), Fall Meet. Suppl., Abstract, SA12A-05.

Rowland, D. E., and J. R. Wygant (1998), Dependence of the large-scale, inner magnetospheric electric field on geomagnetic activity, *J. Geophys. Res.*, *103*, 14,959.

Shiokawa, K., et al. (1998), High-speed ion flow, substorm current wedge, and multiple Pi 2 pulsations, *J. Geophys. Res.*, *103*, 4491.

Siscoe, G. L., and H. E. Petschek (1997), On storm weakening during substorm expansion phase, *Ann. Geophys.*, *15*, 211.

Smith, P. H., and R. A. Hoffman (1973), Ring current particle distributions during the magnetic storms of December 16–18, 1971, *J. Geophys. Res.*, *78*, 4731.

Tsyganenko, N. A. (1989), A magnetospheric magnetic field model with the warped tail current sheet, *Planet. Space Sci.*, *37*, 5.

Tsyganenko, N. A., and M. I. Sitnov (2005), Modeling the dynamics of the inner magnetosphere during strong geomagnetic storms, *J. Geophys. Res.*, *110*, A03208, doi:10.1029/2004JA010798.

Vallat, C., et al. (2004), First comparisons of local ion measurements in the inner magnetosphere with energetic neutral atom magnetospheric image inversions: Cluster-CIS and IMAGE-HENA observations, *J. Geophys. Res.*, *109*, A04213, doi:10.1029/2003JA010224.

Weimer, D. R., D. M. Ober, N. C. Maynard, M. R. Collier, D. J. McComas, N. F. Ness, C. W. Smith, and J. Watermann (2003), Predicting interplanetary magnetic field (IMF) propagation delay times using the minimum variance technique, *J. Geophys. Res.*, *108*(A1), 1026, doi:10.1029/2002JA009405.

Wilken, B., et al. (2001), First results from the RAPID imaging energetic particle spectrometer on board Cluster, *Ann. Geophys.*, *19*, 1355.

P. C. Brandt, H. Korth, A. T. Y. Lui, S. Ohtani, and Y. Zheng, Johns Hopkins University Applied Physics Laboratory, 11100 Johns Hopkins Road, Laurel, MD 20723-6099, USA. (ohtani@jhuapl.edu)

L. G. Blomberg, Royal Institute of Technology, Stockholm, SE-10044 Sweden.

H. U. Frey, Space Sciences Laboratory, University of California, Berkeley, 7 Gauss Way, Berkeley, CA 94720-7450, USA.

M. G. Henderson, Los Alamos National Laboratory, MS D466, Los Alamos, NM 87545, USA.

E. A. Lucek, Blackett Laboratory, Imperial College, London, SW7 2BW, UK.

H. J. Singer, NOAA Space Environment Center, 5271 E Euclid Avenue, Boulder, CO 80303-0000, USA.

J. M. Weygand, Institute of Geophysics and Planetary Physics, University of California, Los Angeles, 3845 Slichter Hall, Los Angeles, CA 90095-1567, USA.

Q. Zong, Center for Atmospheric Research, University of Massachusetts Lowell, 600 Suffolk Street, Lowell, MA 01854-0000, USA.